Crystallization Behavior and Crystallization Kinetic Studies of Isotactic Polypropylene Modified by Long-Chain Branching Polypropylene

Qing-Lin Ni,[1,2] Jia-Qi Fan,[1] Jin-Yong Dong[1]

[1]*Chinese Academy of Sciences Key Laboratory of Engineering Plastics, Joint Laboratory of Polymer Science and Materials, Institute of Chemistry, Chinese Academy of Sciences, Beijing 100190, China*
[2]*Graduate University of Chinese Academy of Sciences, Beijing 100049, China*

Received 21 December 2008; accepted 5 March 2009
DOI 10.1002/app.30363
Published online 2 July 2009 in Wiley InterScience (www.interscience.wiley.com).

ABSTRACT: In this article, we discuss the crystallization behavior and crystallization kinetics of isotactic polypropylene (iPP) modified by long-chain-branching (LCB) high-melt-strength iPP over a wide composition range, that is, LCB-iPP from 10 to 50 wt %. Over the entire range we investigated, the presence of LCB-iPP accelerated crystallization in both the isothermal crystallization process and nonisothermal crystallization process, even when the LCB-iPP content was as low as 10%, and both crystallization processes were enhanced more significantly as the LCB-iPP content increased. Hoffman–Lauritzen theory analysis revealed that the fold-free energy decreased effectively with the occurrence of the LCB structure, although the growth rate of spherulites was depressed, as shown by polarized optical microscopy. Meanwhile, the regime III–regime II transition temperature was about 15° higher for all of the LCB-iPP compositions than that of iPP because the LCB structure reduced the mobility of the polypropylene chains. Furthermore, the γ-form crystal structure was favored by LCB compared to the β form, which was supported by wide-angle X-ray diffraction. © 2009 Wiley Periodicals, Inc. J Appl Polym Sci 114: 2180–2194, 2009

Key words: blends; branched; crystallization; polypropylene (PP)

INTRODUCTION

Isotactic polypropylene (iPP) produced by Ziegler–Natta catalysts or by metallocene catalysts has many desirable and beneficial properties, such as a low density, high stiffness, and excellent chemical resistance and thermal stability. Because of its outstanding functional characteristics and low material costs, polypropylene (PP) has been considered as a substitute for other thermoplastic materials in industrial applications.[1] However, iPP is a linear polymer, which exhibits a low melt strength and weak strain-hardening behavior, so these limitations restrict its use in applications such as thermoforming, foaming, and blow molding. The introduction of long-chain branching (LCB) onto the PP backbone is supposed to be the most effective way to improve its melt strength. There are several possible routes for preparing branching PP, such as irradiation,[2,3] reactive extrusion (REX),[4–6] and polymerization.[7,8]

Yoshii et al.[3] and Krause et al.[2] obtained LCB-PP by irradiating the polymer in the solid state and molten state, respectively. The irradiated PP was found to exhibit obvious melt strain hardening. With increasing irradiation dose, the degree of LCB was increased, but the molecular weight decreased markedly.

Langston et al.[8] prepared LCB-PP via the combination of *rac*-dimethylsilyl-*bis*(2-methyl-4-phenyl-indenyl)zirconium dichloride/methyl aluminoxane catalyst and a *p*-(3-butenyl)styrene (T-reagent). Ye and Zhu[9] synthesized LCB-PP by using tandem catalysis. LCB-PP with a well-defined structure can be obtained by polymerization. The structure of LCB-PP varies according to the methods used. For polyethylene, two kinds of LCB structure exist: treelike and starlike; this could also be assumed for LCB-PP.

REX processes have been used in various types of modification because of their efficiency and economic advantages. Wang et al.[4] prepared branching PP by using REX with peroxide and pentaerythritol triacrylate (PETA). Different concentrations of peroxide and PETA were studied. Low concentrations of PETA and peroxide should be used to minimize the formation of macrogels. Lagendijk et al.[5] prepared LCB-PP by using different types of peroxydicarbonates (PODIC). The efficiency of PODIC with various structures for the LCB modification of PP was evaluated, and the results show that PODIC with nonlinear or large linear alkyl groups had the best effect. Graebling[6] introduced disulfide as a coagent to the REX process. The thiuram disulfide induced a

Correspondence to: J.-Y. Dong (jydong@iccas.ac.cn).
Contract grant sponsor: the National Science Foundation of Chian; contract grant number: 20734002.

decrease in the instantaneous concentration of free radicals, favored the branching, and limited the effect of β scission.

LCB-PP shows more significant strain hardening, a higher elasticity, and faster crystallization compared to linear PP.[10–13] Because of the high costs of LCB-PP, there is growing interest in investigations on blends of linear and LCB-PPs. It was found that the foaming behavior of linear PP could already be improved with respect to higher expansion ratios and reduced cell coalescence by the addition of LCB-PP at contents of 20–30 wt %.[14]

The crystallization behavior of crystalline polymers is greatly influenced by the molecular structure and crystallization conditions. LCB-PP exhibits unique crystallization behavior in terms of a shorter crystallization time and varied crystalline morphologies as compared to linear PP.[15] There have been a few studies on the crystallization of grafted PP and LCB-PP. It is widely accepted that grafted PP partly acts as a nucleating agent for the matrix and accelerates the crystallization rate.[16] Wei et al.[17] found that LCB-PP exhibited a higher overall crystallization rate compared with the linear iPP in the isothermal crystallization process and the reverse result in the nonisothermal process. They attributed this phenomenon to the fact that the key factor that controlled the overall crystallization rate was changed during the two crystallization processes. On the crystal lattice level, iPP exhibits different morphological forms, α, β, and γ, which are distinguished by the arrangement of the chains.[18] The most commonly observed crystal form is the monoclinic α form. Su et al.[19] found that LCB-PP crystallized from the melt as a mixture of α and γ forms. The content of the γ form increased with increasing crystallization temperature (T_c) until it reached a maximum value, and the crystallization of the γ form was favored by the presence of the LCB structure. Agarwal et al.[20] studied the shear-induced crystallization of LCB-PP, and they found that the γ-form crystal was independent of LCB level and induced by regional defects of the chain and shear flow.

LCB-PP is usually used with iPP by melt blending in the foaming. The crystallization behavior plays an important role in this process as does the rheological behavior. So it is important to investigate the crystallization behavior of LCB-PP blends that are rarely reported, although a few studies have been done on the LCB-PP, as mentioned previously. Wang et al.[21] recently investigated the crystallization behavior and crystal morphology of linear/LCB-PP blends. They found that the melt strength and strain rate durability of the blends were obviously enhanced, the nucleation and overall crystallization rates were increased, and T_c was raised after incorporation of LCB-PP into Linear PP. However, the kinetics process was not discussed.

In this article, we discuss the crystallization behavior and crystallization kinetics of linear iPP modified over a wide composition range (10–50 wt %) by a LCB-iPP rendered by a controlled radical branching process that effectively minimized degradation and crosslinking side reactions. Both the isothermal and nonisothermal crystallization processes were studied. An Avrami equation and a nonisothermal crystallization kinetics equation were used for the analysis. The crystal morphology of the polymers was studied by polarized optical microscopy (POM).

EXPERIMENTAL

Sample preparation

LCB-iPP was prepared by REX with peroxide, a polyfunctional monomer, and thiuram disulfide in a TSE-30A intermeshing corotating twin-screw extruder (Nanjing Ruiya Polymer Processing Equipment Co. Ltd., Nanjing, China), with a 40 : 1 length-to-diameter ratio. The screw rotating speed was 150 rpm, which corresponded to the half-time of peroxide. The temperature was set to 170°C for the first zone and 200°C for the die. The extrudates were cooled in water and then palletized. The details of the preparation process were discussed in ref. 6.

The iPP (F401) was supplied by CNPC LanZhou Chemical Co. (LanZhou, China). The free-radical initiator was 2,5-dimethyl-2,5-di(*tert*-butyl peroxy)hexane, the polyfunctional monomer was trimethylolpropane triacrylate, and the sulfide compound was tetraethyl thiuram disulfide. They were all from Aldrich and were used as received.

Blends of the iPP with 10, 20, 30, 40, and 50 wt % LCB-iPP were prepared in a twin-screw extruder equipped with corotating screws, a water cooling bath, and a pelletizer. The extrusion was conducted at a temperature of 200°C and a rotational speed of 100 rpm. The stabilizer B215 was added to avoid degradation during the blending process. According to ref. 14, with a content of LCB-PP up to 50 wt %, a deviation of the zero-shear-rate viscosity from the logarithmic mixing rule was found, and this referred to a disentanglement of the LCB fraction of molecules during the blend extrusion process.

Rheological measurements

Rheological analysis was carried out with a TA AR-2000 rheometer (New Castle, Delaware). The frequency range was 0.01–100 Hz, and the temperature was 190°C. Measurements of the dynamic viscosity were performed with a parallel-plate fixture (diameter = 25 mm) with a gap distance of 1 mm, and the strain was kept at 5% to ensure line viscoelasticity. The measurements were conducted under a dry nitrogen environment to prevent degradation.

Differential scanning calorimetry (DSC)

Thermal analysis of all of the samples was carried out with a PerkinElmer DSC-7 (Waltham, Massachusetts) calibrated with indium. Samples for isothermal and nonisothermal crystallization were first heat-treated at 200°C for 5 min to completely eliminate the thermal history and then fast cooled either to a desired temperature for isothermal crystallization or directly to room temperature at different cooling rates (ϕ's). The weights of all of the samples used for DSC measurements were controlled in the range 2.0–4.0 mg, and each sample was used only one time. All scans were performed under a dry nitrogen environment to prevent the occurrence of oxidation.

POM

An Olympus BH-2 (Olympus America Inc, Center Valley, PA) optical microscope equipped with a Linkam LTS 350 (Linkam Scientific Instruments, Waterfield, UK) hot stage was used under a crossed polarizer. We prepared samples suitable for POM study by pressing them between two glass slides at 200°C. The prepared samples were heat-treated at 200°C for 5 min and rapidly cooled to the desired temperature for isothermal crystallization study.

Wide-angle X-ray diffraction (WAXD)

All WAXD experiments were performed at room temperature with a Rigaku D/max-2500 (Rigaku Corporation, Tokyo, Japan) operated at 40 kV and 150 mA. The experiments were performed with a 2θ range of 5–30° and a scanning rate of 2°/min. The samples for measurement were prepared with the Linkam LTS 350 hot stage. They were compressed into films first, then heat-treated at 200°C for 5 min, and subsequently cooled directly to 130°C for isothermal crystallization for 2 h.

RESULTS AND DISCUSSION

Characterization of the samples

The dynamic shear viscosity of the LCB-iPP was significantly higher than that of the iPP within the measured frequency range [Fig. 1(a)]. As expected, an increasing complex viscosity in the low-frequency range with increasing amount of LCB-iPP was found for the blend with high concentrations of LCB-iPP, which was attributed to the increasing amount of LCB. The only exception was the blend with 10% LCB-iPP. The complex viscosity in the low-frequency range was controlled by two factors: one was the entangled network among the molecular chain, and the other was the molecular weight. Although the antioxidant was added, there still was a little degradation during the extrusion process; as a result, the molecular weight decreased a little. In addition, the entangled network was not obvious with low concentrations of LCB-iPP. Consequently, the complex viscosity of the blend with 10% LCB-iPP was lower than that of the pure iPP. The storage modulus [Fig. 1(b)] in the low-frequency range is also an important parameter for characterizing the elasticity of a polymer melt, and it had the same regularity with the complex viscosity: the storage modulus increased in the low-frequency range with increasing amount of LCB-PP in the compositions.

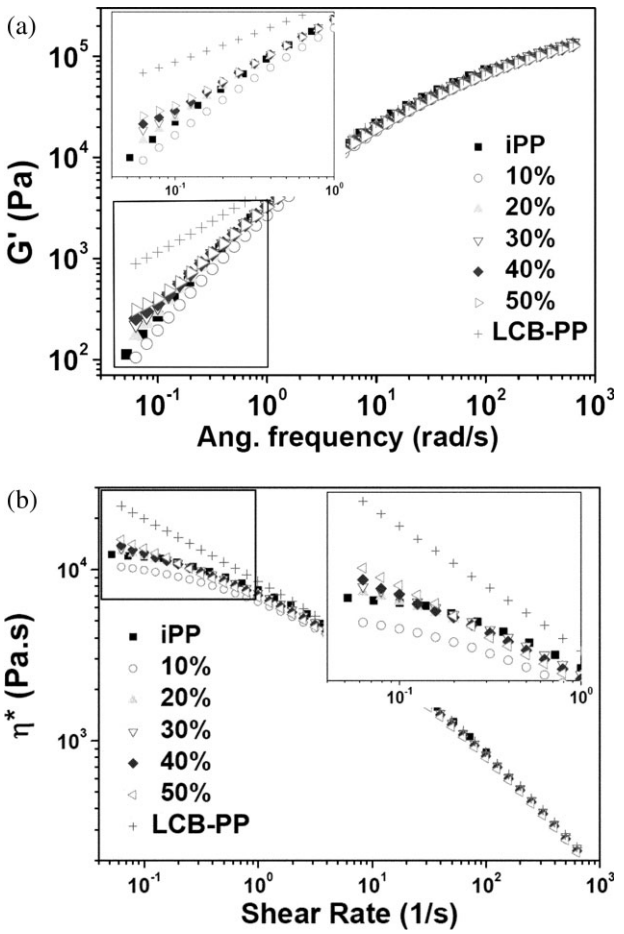

Figure 1 Rheological curves for all of the samples: (a) dynamic modulus (G') and (b) shear viscosity (η^*) versus frequency.

The zero-shear viscosity (η_0) was determined by creep testing, and it followed this relationship:

$$\eta_0 = \lim_{t\to\infty} \frac{t}{J(t)} \quad (1)$$

The content of the branched fraction (B_n) was calculated according to ref. 22. The characteristic data of all of the samples are listed in Table I.

Crystallization behavior

Crystal structure. PP is capable of crystallizing in three polymorphic forms, α (monoclinic), β (pseudohexagonal), and γ (triclinic), depending on the composition of

TABLE I
Characteristic Data of All of the Samples

Material	Melt flow index (g/10 min)	Melting temperature (°C)	T_c (°C)	η_0 ($\times 10^{-4}$ Pa s)	B_n
iPP	2.5	163	113.77	1.45	—
10%	2.9	164	123.77	1.21	—
20%	2.3	165	124.48	1.69	0.08
30%	2.2	164	125.28	1.84	0.13
40%	1.8	164	125.28	2.47	0.29
50%	1.8	164	125.84	2.66	0.33
LCB-PP	0.32	165	127.62	5.35	0.73

PP and the crystallization conditions. The WAXD patterns of all of the samples are shown in Figure 2. The diffraction peaks at 14.0, 16.8, 18.5, 21.0, and 21.8° corresponded to α (110), α (040), α (130), and overlapping α (111) and α (131) reflections, respectively, whereas the diffraction peaks located at 16.1 and 20.1° belonged to the β (300) and γ (117) planes. We found that the α form was the predominant crystal in all of the samples, and there was a little β crystal in iPP and the 10% blends. As the amount of LCB-iPP in the blends increased, the β crystals disappeared, and a small amount of γ crystals turned up.

β-Phase spherulites were obtained sporadically when iPP was crystallized in the 128–132°C temperature range. Although β-iPP is metastable relative to α-iPP, the growth rate of β spherulites is up to 70% faster than that of α spherulites. The introduction of the LCB structure may have reduced the mobility of the PP molecular chains, which led to the disappearance of β crystals.

The most peculiar iPP polymorph is the γ crystal, which was identified in 1961 by Addink and Beitema,[23] who immediately related it to the presence of short chains. The formation of the γ crystal is favored by the presence of stereodefects and regiodefects. The scission and recombination of molecular chains occurred in the LCB-iPP preparation process, which may have led to regiodefects.

POM analysis

The spherulite growth process was observed with POM. Figure 3 illustrates the spherulite growth process of iPP, LCB-iPP, and their blends at 130°C. The spherulite radius for each sample was linearly proportional to the crystallization time (Fig. 4). From the slope, we found that the growth rate of iPP was faster than that of LCB-iPP and their blends. This was explained by the differences in chain mobility. The growth rate of spherulites depended on the activation energy (ΔE), which was necessary for molecular chains to diffuse into the crystallite lattice, whereas ΔE was influenced by chain structure. The long-side branches may have enhanced the entanglement of molecular chains and reduced the transfer of the chain segments to spherulites. As a result, the crystal growth rate of iPP was faster than that of LCB-PP and the blends.

Crystallization kinetics

Isothermal crystallization

Isothermal crystallization kinetics. The isothermal crystallization kinetics of iPP, LCB-iPP, and their blends were investigated by means of DSC. The isothermal crystallization kinetics were analyzed by the Avrami equation:

$$X(t) = 1 - \exp[-K(T)t^n] \tag{2}$$

where $X(t)$ represents the relative crystallinity at different crystallization times, $K(T)$ is a crystallization rate constant containing the nucleation and growth parameters, and n is an Avrami exponent whose value depends on the mechanism of nucleation and on the form of crystalline growth. $X(t)$ can be calculated according to the following equation:

$$X(t) = \frac{Q_t}{Q_\infty} = \frac{\int_0^t [dH(t)/dt]dt}{\int_0^\infty [dH(t)/dt]dt} \tag{3}$$

where the $dH(t)/dt$ is the rate of heat evolution and Q_t and Q_∞ are the heats generated at time t and

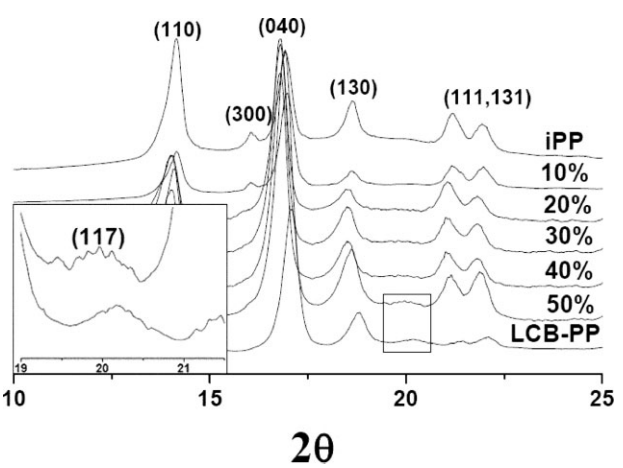

Figure 2 WAXD diffractograms of all of the samples.

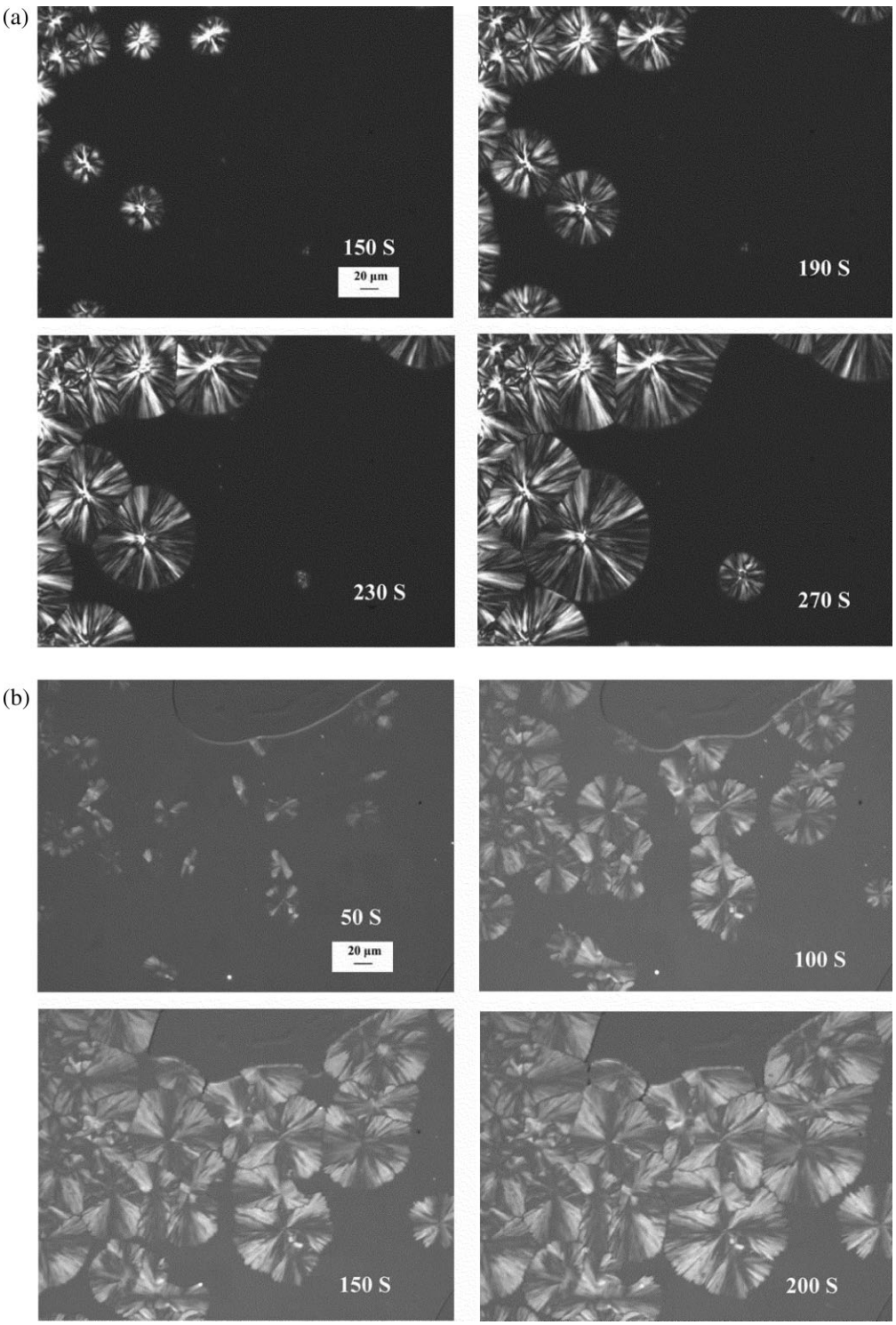

Figure 3 Optical micrographs taken during the isothermal crystallization process at 130°C: (a) iPP and (b) LCB-PP.

infinite time, respectively. Equation (2) can be changed to

$$\log\{-\ln[1 - X(t)]\} = n \log t + \log K(T) \qquad (4)$$

$K(T)$ and n can be determined from the intercept and slope in the plot of $\log\{-\ln[1 - X(t)]\}$ versus $\log t$, respectively.

$X(t)$ as a function of crystallization time at five different temperatures is plotted in Figure 5 for all of the samples. The plot of $\log\{-\ln[1 - X(t)]\}$ versus $\log t$ is shown in Figure 6. We noticed that the Avrami plots of each sample showed good linearity, except for the late crystallization; the deviation may have resulted from the secondary crystallization

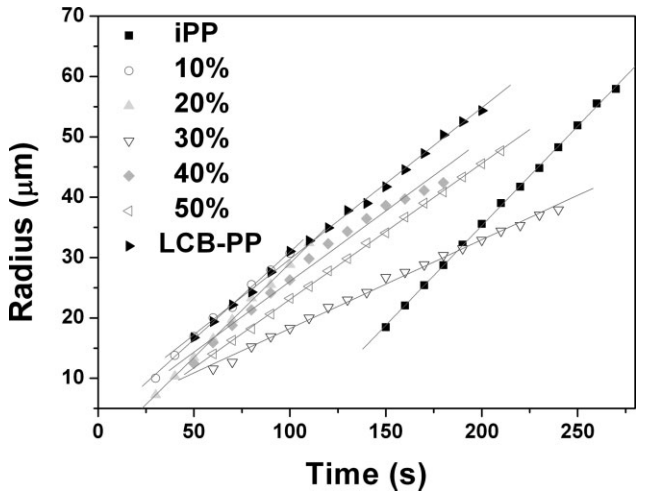

Figure 4 Linear relationship between the spherulite radius and crystallization time of all of the samples during the isothermal crystallization process at 130°C.

caused by the spherulite impingement in the later stage. The kinetic data are listed in Table II.

The crystallization half-time ($t_{1/2}$) is often used to characterize the rate of crystallization. The greater the value of $t_{1/2}$ is, the lower the rate of crystallization is. $K(T)$ and $t_{1/2}$ follow the relationship shown in eq. (5):

$$K(T) = \ln 2 \Big/ t_{1/2}^{n} \tag{5}$$

The deviation was within ±5% when the values of $t_{1/2}$ calculated from eq. (5) was compared with those obtained directly from Figure 5. This means that the Avrami analysis fit the crystallization process well. $t_{1/2}$ of all samples increased with increasing T_c, but the increasing rate of iPP was much faster than LCB-iPP and the blends, which means that the dependence of the crystallization kinetics on the temperature was much weaker for LCB-iPP than for iPP. Meanwhile, $t_{1/2}$ of iPP was much larger than LCB-iPP and the blends at the same T_c. This was ascribed to the heterogeneous nucleation of LCB-iPP, which was less temperature dependent. The decrease in $K(T)$ with increasing T_c again indicated a slower crystallization process of all of the samples at higher T_c's.

The Avrami exponents for iPP were 2.60 ± 0.1 over the T_c range studied. It has been established that spherulitic development arises from an athermal and instantaneous nucleation.[16] The Avrami exponents of the blends of iPP and LCB-iPP were larger than that of linear PP; this also occurred for grafted PP, and this has usually been attributed to a change from instantaneous to sporadic nucleation.[16] However, the Avrami exponents of LCB-iPP were smaller than iPP. The Avrami exponent was related to the nucleation and crystal growth mode. In the system we studied, the LCB structure acted as a heterogeneous nucleating agent and influenced the growth pattern of the crystal; as a result, the crystal of LCB-iPP may have been a mixture that contained rodlike crystals, disklike crystals, and spherulite crystals.

Hoffman–Lauritzen theory. The regime concept for polymer crystallization was first developed by Hoffman and Lauritzen.[24] They used the rate of secondary nucleation and the rate of lateral surface spreading to describe the growth rates of polymer lamellar crystals.

On the basis of Hoffman–Lauritzen theory, the growth rate of polymer spherulites (G) is a function of the undercooling (ΔT) according to the following classic equation:

$$G = G_0 \exp\left[\frac{-U^*}{R(T_c - T_0)}\right] \exp\left[\frac{K_g}{T_c(\Delta T)f}\right] \tag{6}$$

where G_0 is a constant and independent of temperature, U^* is the active energy related to the short diffusion of the crystalline unit across the phase boundary, T_0 is the temperature below which there is no chain motion (usually, $T_0 = T_g - 30$ K, where T_g is the glass-transition temperature), f is the correction factor, K_g is the nucleation constant, and T_m^0 is the equilibrium temperature that was obtained by the Hoffman–Weeks linear extrapolation method.[25] G and f can be calculated, respectively, by eqs. (7) and (8):

$$G = \ln K/n \tag{7}$$

$$f = \frac{2T_c}{T_m^0 + T_c} \tag{8}$$

So, eq. (6) can be transformed into

$$\ln K/n + \frac{U^*}{R(T_c - T_0)} = \ln G_0 - \frac{K_g}{T_c(\Delta T)f} \tag{9}$$

Therefore, K_g can be obtained from the slope in the plot of $\ln(1/t_{1/2}) + U^*/R(T_c - T_0)$ (where R is the universal gas constant) versus $1/T_c\Delta Tf$. K_g also can be expressed as

$$K_g = \frac{nb_0\sigma\sigma_e T_m^0}{\Delta h_f k} \tag{10}$$

$$\sigma = ab_0\Delta h_f \ (a \approx 1)$$

Equation (10) can be transformed into

$$K_g = \frac{n\sigma_e T_{\mathrm{m}}^0}{k} b_0^2 \tag{11}$$

where $n = 4$ for crystallization regimes I and III and $n = 2$ for crystallization II, σ is the lateral surface free energy, σ_e is the fold surface energy, Δh_f is the

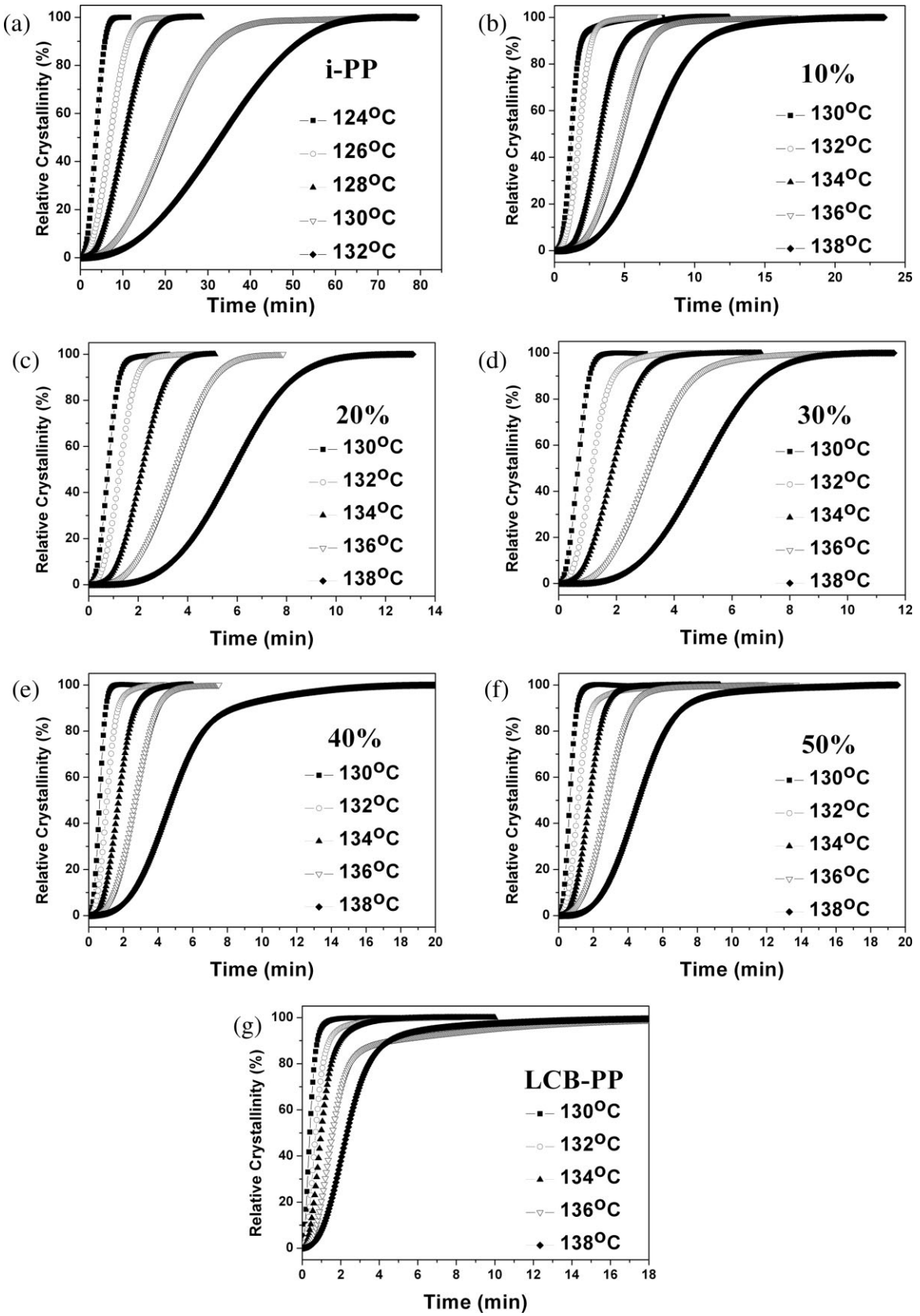

Figure 5 Plots of $X(t)$ versus time for all of the samples during isothermal crystallization at different temperatures.

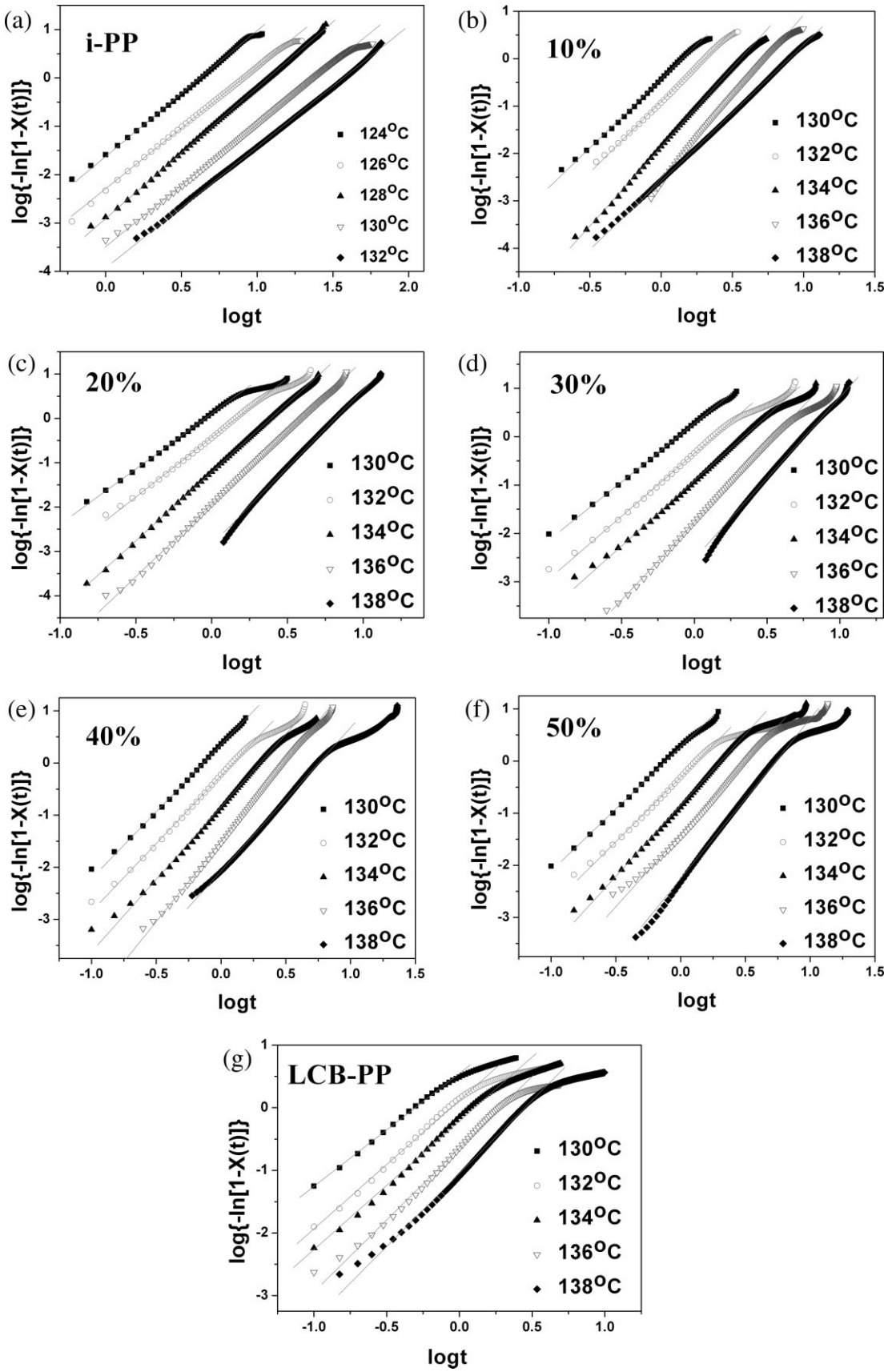

Figure 6 Avrami plots of $\log\{-\ln[1 - X(t)]\}$ versus $\log t$ for all of the samples during isothermal crystallization at different temperatures.

TABLE II
Isothermal Crystallization Kinetic Parameters of All of the Samples

Material	T_c (°C)	$t_{1/2}$ (min)[a]	$t_{1/2}$ (min)[b]	n	log $K(T)$
iPP	118	0.54	0.55	2.68	0.53
	120	1.09	1.08	2.66	−0.25
	122	2.09	2.09	2.47	−0.95
	124	3.72	3.65	2.60	−1.62
	126	6.99	7.04	2.51	−2.29
10%	130	1.20	1.23	2.90	−0.42
	132	1.76	1.78	2.97	−0.91
	134	3.18	3.23	3.33	−1.86
	136	4.75	4.84	3.43	−2.51
	138	6.83	6.96	2.87	−2.58
20%	130	0.79	0.78	2.41	0.091
	132	1.26	1.26	2.65	−0.43
	134	2.15	2.18	3.09	−1.21
	136	3.48	3.54	3.24	−1.94
	138	5.80	6.02	3.62	−2.98
30%	130	0.66	0.66	2.35	0.26
	132	1.15	1.17	2.62	−0.34
	134	1.85	1.90	2.68	−0.91
	136	3.11	3.20	3.17	−1.76
	138	4.94	5.13	3.39	−2.56
40%	130	0.62	0.63	2.57	0.35
	132	1.05	1.06	2.63	−0.23
	134	1.72	1.76	2.80	−0.84
	136	2.69	2.79	3.00	−1.50
	138	4.74	4.92	2.78	−2.08
50%	130	0.64	0.66	2.29	0.24
	132	1.09	1.15	2.43	−0.31
	134	1.74	1.78	2.73	−0.84
	136	2.77	2.82	2.76	−1.40
	138	4.61	4.69	3.18	−2.29
LCB-PP	130	0.40	0.40	1.81	0.55
	132	0.71	0.71	2.17	0.16
	134	1.02	1.00	2.28	−0.15
	136	1.59	1.58	2.42	−0.64
	138	2.35	2.38	2.43	−1.07

[a] $t_{1/2}$ obtained directly from Figure 5.
[b] $t_{1/2}$ calculated by eq. (5).

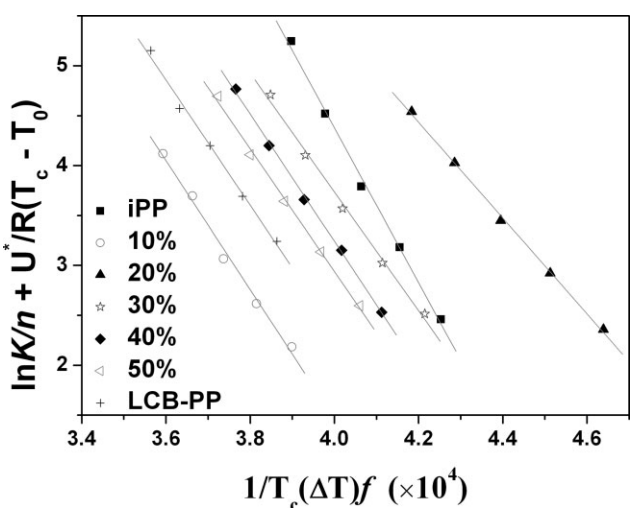

Figure 7 Plot of ln $K/n + U^*/R(T_c - T_0)$ versus $1/T_c\Delta Tf$ for all of the samples.

enthalpy of fusion, k is Boltzmann's constant, and b_0 is the layer thickness. The value of U^*, T_0, and b_0 are 6300 J/mol, 233 K, and 6.56 A, respectively.

The plot of ln $K/n + U^*/R(T_c - T_0)$ versus $1/T_c\Delta Tf$ for all samples are shown in Figure 7. The crystallization behavior of PP usually shows regimes II and III.[26] As shown in Figure 8, the transition for

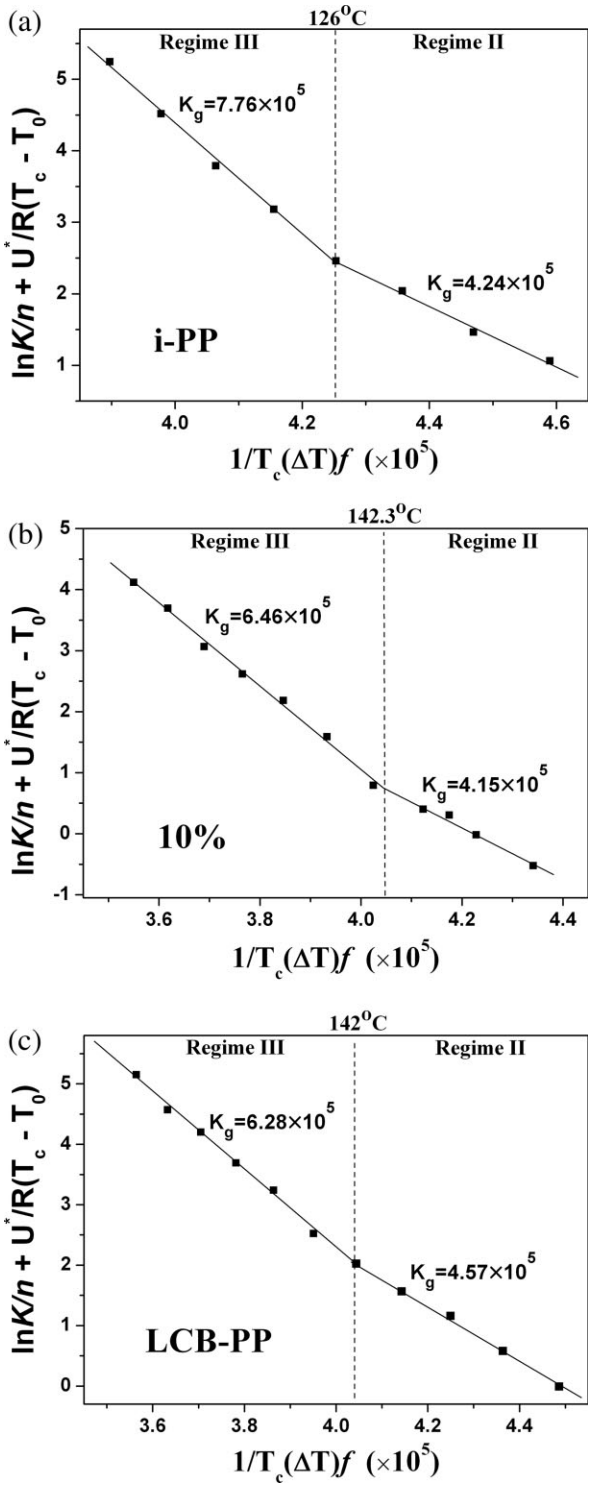

Figure 8 Plot of ln $K/n + U^*/R(T_c - T_0)$ versus $1/T_c\Delta Tf$.

TABLE III
Value of T_m^0, K_g, and σ_e for All of the Samples

Material	T_m^0 (°C)	K_g ($\times 10^{-5}$)	σ_e ($\times 10^3$ J/m^2)
iPP	189.6	7.76	13.5
10%	205.5	6.46	10.8
20%	194.0	4.80	8.24
30%	200.1	5.95	10.1
40%	201.7	6.37	10.8
50%	202.6	6.14	10.4
LCB-PP	206.1	6.28	10.5

iPP that we used occurred at 127°C, and the transition temperature for LCB-iPP and its blends was located around 142°C, which was 15° higher than the transition temperature for iPP that we used. This showed that the T_c range of regime III became broader in the LCB-iPP and its blends. Because the regime transition was controlled by the relative rates of secondary nucleation and layer completion, any factor that affected either of these rates altered the temperature at which the transition occurred. The

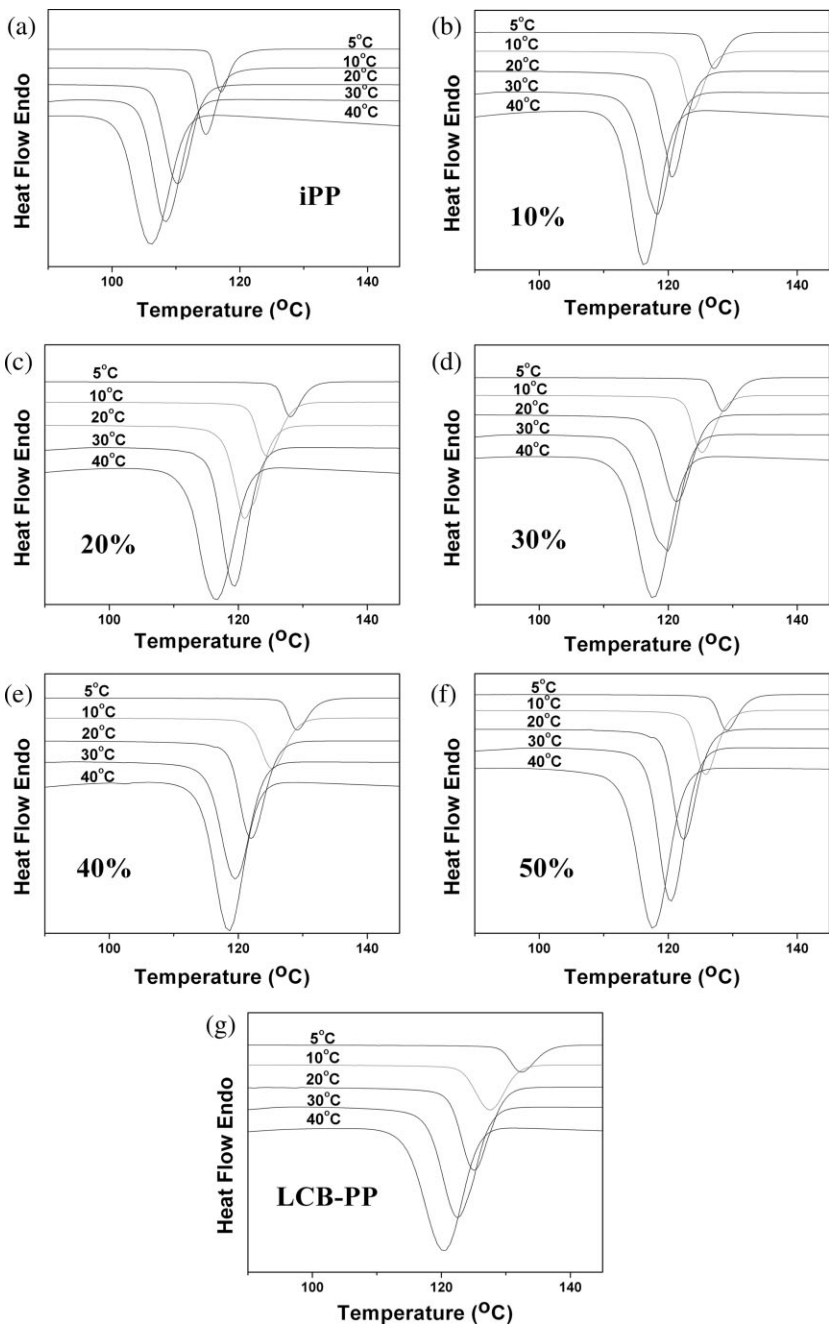

Figure 9 DSC thermogram of all of the samples during nonisothermal crystallization at different ϕ values.

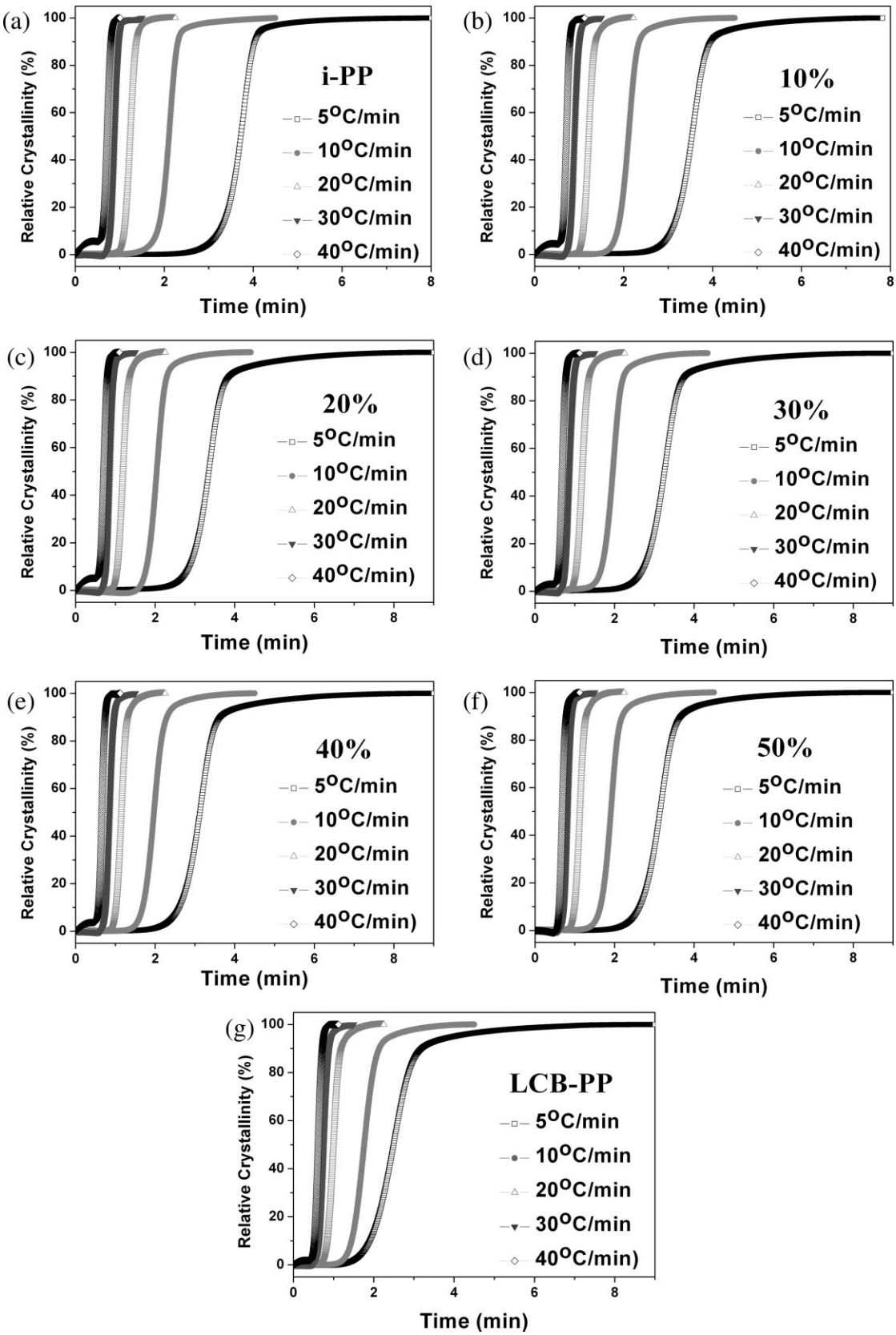

Figure 10 Plots of $X(t)$ versus time for all of the samples during nonisothermal crystallization at different ϕ values.

elimination of reptation by crosslinking or by grafting with relative side groups moved the crystallization inevitably to regime III because the completion of the layer on the growth face required adjacent reentry folding and transport of macromolecular chains over large distances.[27] The LCB structure reduced the mobility and reptation ability of the PP chains, which increased the regime III–regime II transition temperature by 15°.

So, the T_c range that we used for iPP, LCB-iPP, and their blends all belonged to regime III, that is, from 118 to 126°C and from 130 to 138°C, respectively. This also implied that the T_c value should be carefully chosen when PPs with different structures are used, or incorrect conclusions may be reached. The results are listed in Table III. This shows that the σ_e's of LCB-iPP and its blends were lower than those of iPP. We speculated that the LCB structure decreased σ_e effectively. The smaller the fold-free energy of the crystallization surface was, the easier it was for the macromolecular chain to form crystal structures. Therefore, the LCB structure increased the nucleation and overall crystallization rate of PP. The conclusions from Hoffman theory accorded very well with the Avrami analysis.

Nonisothermal crystallization

We also investigated the nonisothermal crystallization process of all of samples because the actual processing of polymers was more likely to proceed under nonisothermal conditions.

Nonisothermal crystallization kinetics. The nonisothermal DSC thermograms of all of samples at five different ϕ's, ranging from 5 to 40°C/min, are shown in Figure 9. We found that the exothermic peak shifted to lower temperatures and became broader with increasing ϕ for all samples. This showed a poor crystallization ability of both samples caused by poor chain mobility at high ϕ.

During the nonisothermal crystallization process, $X(t)$ as a function of temperature (T) can be obtained with the following equation:

$$X(t) = \frac{\int_{T_0}^{T} (dH/dT)dT}{\int_{T_0}^{T\infty} (dH/dT)dT} \quad (12)$$

The crystallization time (t) has the following relationship with T:

$$t = \frac{T_0 - T}{\phi} \quad (13)$$

where T_0 is the onset crystallization temperature and T is the temperature at time t. The plots of $X(t)$ versus t for all of the samples are shown in Figure 10. The $t_{1/2}$ values obtained from Figure 10 are listed in Table IV. As expected, the value of $t_{1/2}$ decreased with increasing ϕ for all of the samples. Furthermore, at a given ϕ, the value of $t_{1/2}$ for LCB-iPP and its blends were lower than that for iPP, which indicated that the LCB structure accelerated the crystallization process.

TABLE IV
Half-Time of All of the Samples from Nonisothermal Crystallization

	ϕ (°C)				
Material	5	10	20	30	40
iPP	3.72	2.11	1.23	0.88	0.71
10%	3.54	2.12	1.22	0.90	0.71
20%	3.35	2.04	1.19	0.86	0.71
30%	3.24	1.96	1.19	0.86	0.69
40%	3.15	1.97	1.15	0.85	0.66
50%	3.15	1.90	1.13	0.82	0.69
LCB-PP	2.49	1.76	1.00	0.75	0.62

The Avrami equation was extended to the nonisothermal crystallization process by Jeziorny,[28] who defined $\lg Z_c = \lg(Z_t/\phi)$, where Z_t is the crystallization rate constant; Z_c is the modified crystallization rate constant with regard to ϕ. Considering the effect of a cooling (or heating) effect, Ozawa[29] modified the Avrami equation as follows:

$$1 - X(T) = \exp[-K(T)/\phi^m] \quad (14)$$

Mo et al.[30] tried to describe the nonisothermal crystallization process more precisely by combining the expanded Avrami equation with the Ozawa equation to form a new equation:

$$\ln Z_t + n \ln t = \ln K(T) - m \ln \phi \quad (15)$$

By rearrangement at a given $X(t)$

$$\ln \phi = \ln F(T) - \alpha \ln t \quad (16)$$

where $F(T) = [K(T)/Z_t]^{1/m}$ refers to the cooling rate chosen to attain a certain degree of crystallinity at a unit crystallization time, where $\alpha = n/m$, that is, the ratio of n to the Ozawa exponent m. From eq. (16), we developed a series of linear plots at different crystallinities, as shown in Figure 11. The kinetic parameter $F(T)$ and α were determined from the intercept and slope of the lines, and the results are listed in Table V. $F(T)$ increased gradually with increasing $X(t)$, whereas α remained almost constant. The $F(T)$ values of iPP were lager than those of LCB-iPP over the chosen $X(t)$ range, but the distinction of $F(T)$ between iPP and LCB-iPP at the same crystallinity decreased with increasing $X(t)$; the same consequence occurred between iPP and the blends. This result implies that the nucleation at the early stage determined the overall crystallization rate, and the LCB-iPP had no advantage in the chain diffusion process at the later stage. This result was the

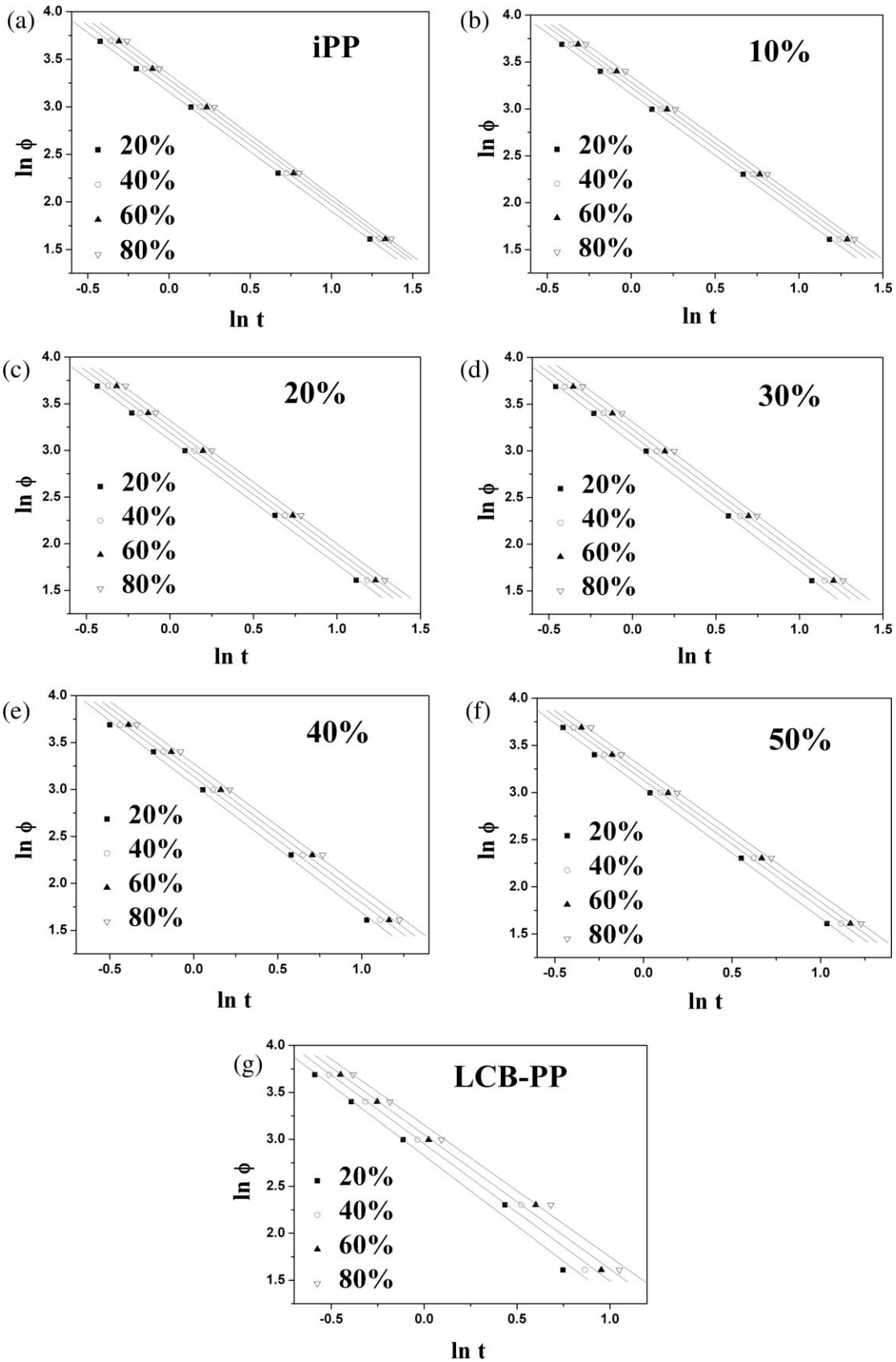

Figure 11 Plots of ln ϕ versus ln *t* for all of the samples.

opposite of the conclusion from Zeng et al.;[17] it may lie on the difference between the samples that we used. The branching density of LCB-PP that Zeng et al.[17] used may have been very small; as a consequence, the nucleation effect was not so obvious during the nonisothermal process. In addition, the samples that Zeng et al.[17] used and the samples we used were prepared by different methods, so the LCB structures that were created by these different methods may have been somewhat different.

Kissinger method. It is known that the crystallization of a polymer is controlled by two factors: one is the dynamic factor, which is related to ΔE for the transport of crystalline units across the phase, and the other is the static factor, which is related to the free-energy barrier for nucleation. Considering the variation of peak temperature (T_p) with ϕ, we evaluated ΔE of nonisothermal crystallization from the Kissinger method:[31]

$$\frac{d[\ln(\phi/T_p^2)]}{d(1/T_p)} = \frac{-\Delta E}{R} \tag{17}$$

Figure 12 shows the plots of all of the samples, and ΔE was obtained from their slopes. The results of ΔE are listed in Table V. The value of ΔE for iPP

TABLE V
Nonisothermal Crystallization Kinetic Parameters of All of the Samples

Material	X_t (%)	α	$F(T)$	ΔE (kJ/mol)
iPP	20	1.25	23.460	237.5
	40	1.26	25.214	
	60	1.26	26.727	
	80	1.27	28.293	
10%	20	1.30	23.519	257.7
	40	1.30	25.284	
	60	1.29	26.628	
	80	1.30	28.363	
20%	20	1.33	22.448	254.7
	40	1.32	24.258	
	60	1.32	25.877	
	80	1.32	27.666	
30%	20	1.36	21.822	254.8
	40	1.34	23.705	
	60	1.34	25.366	
	80	1.34	27.340	
40%	20	1.36	21.147	261.0
	40	1.34	23.007	
	60	1.34	24.607	
	80	1.33	26.427	
50%	20	1.38	21.048	248.3
	40	1.36	22.885	
	60	1.35	24.307	
	80	1.34	26.107	
LCB-PP	20	1.50	16.876	250.1
	40	1.46	19.168	
	60	1.43	21.122	
	80	1.40	23.399	

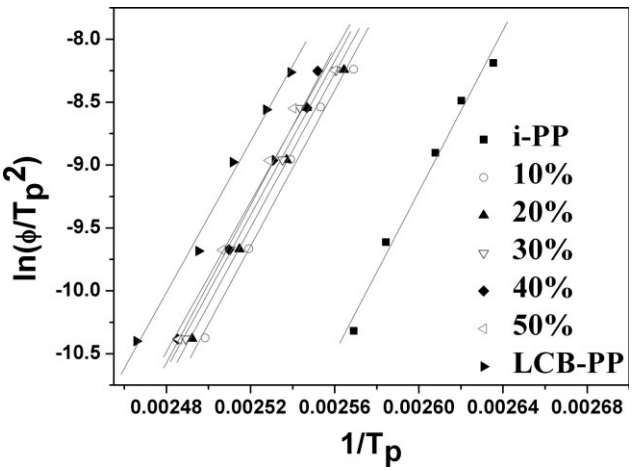

Figure 12 Plot of $\ln(\phi/T_p^2)$ versus $1/T_p$ for all of the samples.

was lower than that for LCB-iPP and the blends; this indicated that the presence of LCB hampered the transfer of chain segments from the melt to the crystal growth surface. This coincided with the kinetics results discussed previously.

CONCLUSIONS

The crystallization behaviors and crystallization kinetics of iPP, LCB-iPP and their blends were studied by varied methods. The presence of a LCB structure decreased the fold-free energy of nucleation and increased ΔE for the transport of crystalline units across the phase. The crystallization characteristics of iPP were greatly changed by the addition of LCB-iPP; even the blend composed of 10% LCB-iPP showed more characteristics of LCB-iPP than of iPP, such as an increased regime II–regime III temperature, a decreased fold-free energy, and an accelerated crystallization process, and this became more pronounced as the LCB-iPP content was increased.

The Avrami equation and Hoffman–Lauritzen theory were used to analyze the isothermal crystallization behavior. The results showed that the LCB structure was effective not only in increasing the nucleus number but also in decreasing the fold-free energy and accelerating the growth rate of crystallization. The change in the Avrami exponent showed that the LCB structure may have affected the crystal growth mode. The LCB structure reduced the mobility and reptation ability of the PP chains, which increased the regime III–regime II transition temperature by 15°.

During the nonisothermal crystallization process, at various ϕ values, the exothermic peaks of LCB-iPP and the blends distinctly shifted to higher temperatures compared with that of linear PP. A kinetic model based on Mo et al.'s work[29] and the Kissinger

method[30] was used to analyze the nonisothermal crystallization behavior. The results show that the value of ΔE for iPP was lower than that for LCB-iPP and the blends; this indicated that the presence of LCB hampered the transfer of chain segments from the melt to the crystal growth surface, which was consistent with POM observation.

References

1. Gotsis, A. D.; Zeevenhoven, B. L. F.; Hogt, A. H. Polym Eng Sci 2004, 44, 973.
2. Krause, B.; Stephan, M.; Volkland, S.; Voigt, D.; Haussler, L.; Dorschner, H. J Appl Polym Sci 2006, 99, 260.
3. Yoshii, F.; Makuuchi, K.; Kikukawa, S.; Tanaka, T.; Saitoh, J.; Koyama, K. J Appl Polym Sci 1996, 60, 617.
4. Wang, X. C.; Tzoganakis, C.; Rempel, G. L. J Appl Polym Sci 1996, 61, 1395.
5. Lagendijk, R. P.; Hogt, A. H.; Buijtenhuijs, A.; Gotsis, A. D. Polymer 2001, 42, 10035.
6. Graebling, D. Macromolecules 2002, 35, 4602.
7. Weng, W. Q.; Hu, W. G.; Dekmezian, A. H.; Ruff, C. J. Macromolecules 2002, 35, 3838.
8. Langston, J. A.; Colby, R. H.; Chung, T. C. M.; Shimizu, F.; Suzuki, T.; Aoki, M. Macromolecules 2007, 40, 2712.
9. Ye, Z. B.; Zhu, S. P. J Polym Sci Part A: Polym Chem 2003, 41, 1152.
10. Auhl, D.; Munstedt, H.; Lappan, U. In Proceedings of the 6th European Conference on Rheology, Erlangen, Germany; 2002; p 371.
11. Hingmann, R.; Marczinke, B. L. J Rheol 1994, 38, 573.
12. Kurzbeck, S.; Oster, F.; Munstedt, H. J Rheol 1999, 43, 359.
13. Sugimoto, M.; Tanaka, T.; Masubuchi, Y.; Takimoto, J.; Koyama, K. J Appl Polym Sci 1999, 73, 1493.
14. Stange, J.; Uhl, C.; Munstedt, H. J Rheol 2005, 49, 1059.
15. Tian, J. H.; Yu, W.; Zhou, C. X. J Macromol Sci Phys 2006, 45, 969.
16. Seo, Y.; Kim, J.; Kim, K. U.; Kim, Y. C. Polymer 2000, 41, 2639.
17. Zeng, W.; Liu, J. C.; Zhou, J. F.; Dong, J. Y.; Yan, S. K. Chin Sci Bull 2008, 53, 188.
18. Thomann, R.; Semke, H.; Maier, R. D.; Thomann, Y.; Scherble, J.; Mulhaupt, R.; Kressler, J. Polymer 2001, 42, 4597.
19. Su, Z. Q.; Wang, H. Y.; Dong, J. Y.; Zhang, X. Q.; Dong, X.; Zhao, Y.; Yu, J.; Han, C. C.; Xu, D. F.; Wang, D. J. Polymer 2007, 48, 870.
20. Agarwal, P. K.; Somani, R. H.; Weng, W. Q.; Mehta, A.; Yang, L.; Ran, S. F.; Liu, L. Z.; Hsiao, B. S. Macromolecules 2003, 36, 5226.
21. Wang, X. D.; Zhang, Y. X.; Liu, B. G.; Du, Z. J.; Li, H. Q. Polym J 2008, 40, 450.
22. Tsenoglou, C. J.; Gotsis, A. D. Macromolecules 2001, 34, 4685.
23. Addink, E. J.; Beitema, J. Polymer 1961, 2, 185.
24. Lauritzen, J. I.; Hoffman, J. D. J Appl Phys 1973, 44, 4340.
25. Xu, J. N.; Srinivas, S.; Marand, H.; Agarwal, P. Macromolecules 1998, 31, 8230.
26. Cheng, S. Z. D.; Janimak, J. J.; Zhang, A. Macromolecules 1990, 23, 298.
27. Karger-Kocsis, J. Polypropylene—An A–Z Reference; Springer-Verlag: Berlin, 1999.
28. Jeziorny, A. Polymer 1978, 19, 1142.
29. Ozawa, T. Polymer 1971, 12, 150.
30. Liu, T. X.; Mo, Z. S.; Wang, S. G.; Zhang, H. F. Polym Eng Sci 1997, 37, 568.
31. Kissinger, H. E. J Res Natl Bur Stand 1956, 57, 217.